

Facile charge transport in FeN_x/Mo₂N/CNT nanocomposites for efficient hydrogen evolution reactions[†]

KASINATH OJHA^a, SHIVALI BANERJEE^a and ASHOK K GANGULI^{a,b,*}

^aDepartment of Chemistry, Indian Institute of Technology Delhi, Hauz Khas, New Delhi 110 016, India

^bInstitute of Nano Science and Technology, Phase-10, Sector-64, Mohali, Punjab 160 062, India

E-mail: ashok@chemistry.iitd.ac.in

MS received 2 February 2017; revised 7 May 2017; accepted 12 May 2017

Abstract. Molybdenum based materials are gaining importance as electrocatalysts for hydrogen evolution reaction because of their low cost and good electrocatalytic efficiency. Introducing iron nitride with molybdenum nitride as a composite results in efficient hydrogen evolution activity with current density of ~ 120 mA/cm² at -400 mV vs. RHE. The nanocomposites were characterized using powder XRD, Scanning Electron Microscopy (SEM), Transmission Electron Microscopy (TEM), Electron Diffraction, Thermogravimetric Analysis and FTIR Spectroscopy. The electrochemical investigations suggest that the electrocatalytic activity of the composite increases with iron nitride content. The composite exhibits good electrochemical stability upto 42 hours in acidic medium. The hydrogen evolution reaction (HER) follows Volmer-Heyrovsky mechanism where Volmer reaction is the rate determining step.

Keywords. Metal nitride; nanocomposites; hydrogen evolution reaction; N-doped CNTs.

1. Introduction

The hydrogen evolution reaction (HER) is the essential reaction to produce hydrogen fuel from water. Hydrogen produced in this manner can be stored and transported more easily. However, the energy barrier of the reaction to generate hydrogen restricts its overall efficiency of hydrogen production. Efficient production of hydrogen therefore requires efficient catalysts. Unfortunately, the use of the best HER catalyst (*i.e.*, Pt) for renewable H₂ production^{1,2} is restricted due to its scarcity and high cost. These limitations have driven extensive efforts to design and develop non-noble metal based electrocatalysts which are stable under acidic medium, unlike Ni-based HER catalysts which are only stable under alkaline medium.¹ Notable development has been made in the past 3–4 years in acid-stable HER catalysts, resulting in excellent HER activity for transition metal carbides,^{3–5} nitrides,⁶ phosphides,^{7,8} sulfides^{9–12} and borides.^{13,14} However, the most important parameter for HER is the moderate binding of hydrogen atom on the surface of the catalyst. Pt exhibits best HER performance as it has the optimum binding of hydrogen (Pt-H binding energy = -0.33 eV) and all the reactions steps for hydrogen evolution are thermo-neutral.¹⁵

The theoretical investigations find that the d-band of the transition metal contributes to the M-H bond where the d-band center plays the most important role. In ‘Mo’ based compounds, the d-band center is shifted down relative to the Fermi level which enhances the ability of Mo atoms to donate electrons which in-turn decreases the H-binding energy to an optimum energy favourable for hydrogen adsorption on the surface (Volmer process).¹⁶ Molybdenum nitride based nanostructures were reported to be potential electrocatalysts for HER in acidic medium.^{17,18} Matanovic *et al.*, have shown the efficient binding of H₂ and H on different binding sites of γ -Mo₂N where perfect, defect-free surfaces of (100), (101), (111) and surface with defects (111) have higher hydrogen adsorption energies for bridging and fcc binding sites than those of top binding sites.¹⁹ Chen *et al.*, have demonstrated high HER activity of NiMoN_x/C catalyst¹⁶ with overpotential of 78 mV and Tafel slope of 35 mV dec⁻¹. Cao *et al.*, have reported a highly active and stable Co-doped MoN electrocatalyst where ternary Co_{0.6}Mo_{1.4}N₂ is very much effective for HER activity compared to binary δ -MoN.²⁰ Xie *et al.*, have demonstrated the HER activity of atomically thin metallic MoN nanosheets where Mo atoms play the crucial role for transforming protons into hydrogen.¹⁸ Bimetallic nitride systems like Ni-Mo-N catalyst were found to contain a mixture of phase Ni-doped Mo₂N and a

*For correspondence

[†]Dedicated to the memory of the late Professor Charusita Chakravarty.

$\text{Ni}_2\text{Mo}_3\text{N}(\text{Mo}_3\text{Al}_2\text{C}$ -type) phase in which Mo is having valence near to zero and is important for HER activity.¹⁶ Both low electrical resistance and good corrosion resistance are the promising factors for transition-metal nitrides for electrocatalytic applications.²¹

Molybdenum-nitrogen systems have different crystalline phases²² such as α - MoN_x , β - Mo_2N , γ - Mo_2N and δ - MoN . In α -phase, N content is very low (0–1.08%) and maximum concentration of nitrogen (1.08%) has been reported at the eutectic temperature of 1860°C. β -phase has tetragonal structure with nitrogen content of 28.7 to 35% and is stable at low temperature. γ -phase having face centered cubic structure, is formed at high temperature (above 760°C) with nitrogen content of 27–35%. The only stoichiometric phase (δ - MoN) has hexagonal structure and is formed around 1000°C. Along with this, a new phase of Mo-N system has been reported recently²³ where the nitrogen rich phase (MoN_2) adopts a rhombohedral structure, isotopic to MoS_2 .

In this report, iron nitride based Mo_2N composite were synthesized where *in situ* growth of N-doped CNTs were observed. The presence of N-doped CNTs were evident from microscopy and spectroscopic studies. CNTs enhance the overall conductivity of the composites facilitating the charge transfer process at the electrode | electrolyte interface leading to facile HER process. The composites exhibit much higher HER activity compared to bare counterparts.

2. Experimental

2.1 Materials and synthesis

Ammonium Molybdate (CDH chemicals, India), Ferric Nitrate (Fisher scientific, India) and Melamine (CDH chemicals, India) were used without any further purification. Nafion was purchased from Sigma Aldrich. Double distilled water was used in all the experiments.

Molybdenum nitride was prepared by dissolving ammonium molybdate as a source of molybdenum with melamine as a source of nitrogen in double distilled water and stirring the resultant solution at 60–80°C leading to complete dryness. The resultant powdered compound was annealed in the furnace at 600°C for 10 h in Argon atmosphere.

The composites of iron nitride and molybdenum nitride were prepared in a similar way by dissolving ammonium molybdate, melamine and iron(III) nitrate in double distilled water and stirring the resulting solution at 60–80°C leading to complete dryness. The resulting powdered compound was then annealed in the furnace at 600°C for 10 h in Argon atmosphere. The amount of iron(III) salt added was varied as 4.7%; 14%; 42% and 100% (atomic percentage) and the composites

were marked as MN-Fe25, MN-Fe50, MN-Fe75 and Fe100, respectively. The composition of 100% iron does not contain any ammonium molybdate.

2.2 Characterization

Powder X-ray diffraction measurements were carried out on a Bruker D8 Advance. TEM specimens were prepared onto a carbon coated copper grid by drop cast of the nanocomposites dispersion in ethanol and then it was dried in air. The surface morphologies of all the synthesized samples were analyzed using a Field Emission Scanning Electron Microscopy (FEI QUANTA 3D FEG) operating at an accelerating voltage of 10 kV. Thermogravimetric analysis (TGA) of the samples have been carried out using Pyris 1 instrument (Perkin Elmer) operated at 50–900°C at N_2 atmosphere.

2.3 Electrochemical studies

Linear Sweep Voltammetry (LSV), Cyclic voltammetry (CV) and impedance measurements were carried out using an electrochemical workstation (Autolab PGSTAT302N). Hydrogen evolution reactions were studied by using the nanocomposites coated on glassy carbon electrode where Ag/AgCl was the reference electrode and Pt was the counter electrode. A slurry was obtained by sonicating the mixture of 2 mg of the nanocomposite, 20 μL of isopropanol and 20 μL of Nafion. 20 μL of this slurry was carefully drop-casted on the working electrode and dried for 10 min. All the three electrodes were placed in a freshly prepared 0.5 M H_2SO_4 solution. Linear Sweep Voltammetry was carried out at a scan rate of 5 mV/s in the potential range of (0 to -0.6 V). Cyclic voltammetry was carried out at a scan rate of 10 mV/s in the potential range of -0.5 to $+1$ V. Electrochemical impedance spectroscopic measurements were carried out at different applied potentials in the frequency range of 100 kHz to 0.1 Hz at an amplitude of 10 mV. All the potentials were reported with respect to reversible hydrogen electrode (RHE).

3. Results and Discussion

The reaction between ammonium molybdate and melamine at high temperature results in molybdenum nitride formation. Melamine initially produced NH_3 during its condensation above 300°C at furnace²⁴ and then NH_3 reacts with Mo atoms to form Mo_2N . The formation of molybdenum nitride was confirmed from the powder X-ray diffraction studies (Figure 1) where the XRD peaks at 2θ values of 37.69, 43.04, 64.26 and 75.34 are indexed to (112), (200), (220) and (312) crystallographic planes, respectively, corresponding to the β phase of Mo_2N having tetragonal structure (JCPDS 751150). We have introduced iron nitride in composite with Mo_2N . During the synthesis, Fe-salt was added in varying ratio with ammonium molybdate to

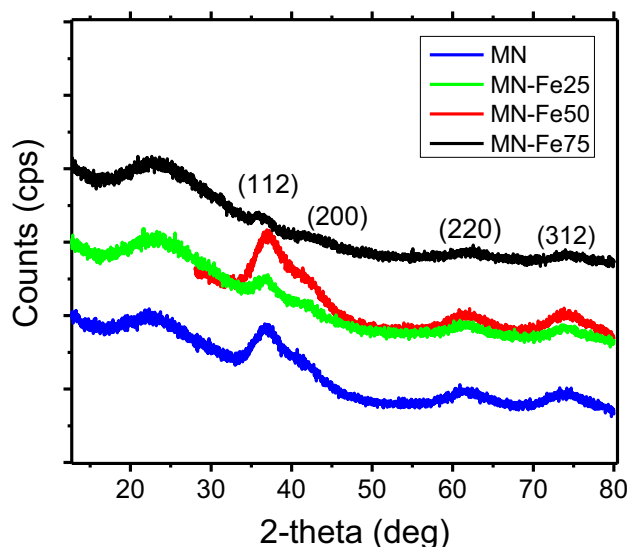
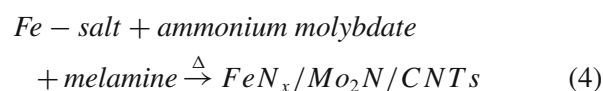
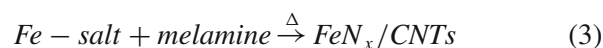
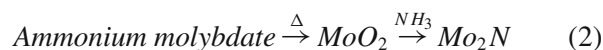
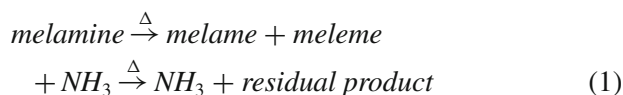


Figure 1. Powder X-Ray diffraction of Mo_2N and its composites.

obtain composites with varying iron nitride content. The reaction between Fe-salt with melamine at $600^\circ C$ in Ar atmosphere leads to the formation of iron nitride and the powder XRD pattern of the iron nitride has been given in Figure S1a (Supplementary Information). FTIR data (Figure S1b in Supplementary Information) of iron nitride suggests the presence of peaks at 1320 cm^{-1} (C-C and C-N), 1613 cm^{-1} (C=C and C=N) and 2042 cm^{-1} (C \equiv C or C \equiv N). This confirms the presence of N-doped CNTs with iron nitride. TGA analysis of the iron nitride system suggests that there are two decomposition temperatures at $550^\circ C$ and $695^\circ C$. Higher decomposition temperature of $695^\circ C$ is due to carbon nanotubes (CNTs). TGA analysis suggests almost 50% weight loss was observed which indicates that $\sim 50\%$ (wt%) of the composite is due to CNTs (Figure S2 in Supplementary Information). The presence of C-N bonds (FTIR) confirms that these are N-doped CNTs. The EDAX studies of the FeN_x system also suggests that the Fe:N ratio is 1:1 (Figure S3a and Table S1 in Supplementary Information). However, presence of N-doped CNTs indicates that iron nitride might have N content (x) lower than 1.

The reaction can be represented as below:



To probe the surface morphology of Mo_2N and iron nitride based Mo_2N nanocomposite, we performed the Field Emission Scanning Electron Microscopy (FESEM) measurements. Figure 2a shows Mo_2N nanoparticles assembled in a rod-like morphology. There are also some broken particles as observed in the SEM image. Interestingly, when Fe ions were introduced in the reaction, instead of the rod morphology of Mo_2N , small particles were observed. Introducing Fe in the system disrupts the rod assembly of Mo_2N particles. In presence of Fe, formation of wire-like structures was observed in the SEM images and the amount of these wire structures increases as we increase Fe content in the composite (Figures 2b–d). These wire-like structures were found to be carbon nanotubes (CNTs). In the SEM images of the composites (Figure 2), the presence of CNTs were clearly evident. Presence of Fe in the reaction systems catalyzes the formation of CNTs during the condensation of melamine. Therefore, these CNTs may be N-doped CNTs as these are produced from melamine. The SEM and TEM images of the Fe100 where iron nitride particles and CNTs were observed homogeneously throughout the sample (Figure S4a, b in Supplementary Information). From the Raman spectrum, it is clear that there are signature bands for CNTs at 1356 cm^{-1} (D band), 1584 cm^{-1} (G band) and RBM bands (Figure S4c in Supplementary Information). There are two different RBM bands at 210 cm^{-1} and 279 cm^{-1} which confirm the presence of CNTs (Figure S4c in Supplementary Information). We have carried out TEM analysis of one of the samples MN-Fe50 where Fe and Mo ratio is 14:86 (Figure 3). It shows the presence of aggregated Mo_2N particles (Figure 3a) and the presence of CNTs were also observed (Figure 3b). Electron diffraction suggests the polycrystalline nature of the nanostructures (Figure 3c). The EDAX analysis shows the presence of Mo and Fe in the composite (Figure 3d). SEM EDAX quantification of these composites were carried out to find out the Fe content in the composites (Figure S3). It suggests that MN-Fe25, MN-Fe50 and MN-Fe75 composites have 6%, 13% and 30% of Fe content, respectively (Table S2 in Supplementary Information). Thermogravimetric analysis (TGA) was carried out in N_2 atmosphere to look at the weight loss of the composites upto $900^\circ C$ (Figure S5a in Supplementary Information). These composites were synthesized at $700^\circ C$ in furnace and still they exhibit very small weight loss ($\sim 2\text{--}5\%$) upto $600^\circ C$. After $600^\circ C$, it shows 10–20% weight loss due to the removal of surface oxide impurities and CNTs. MN-Fe75 composite exhibits maximum weight loss indicating that it contains maximum amount of CNTs in composites. FTIR studies of the composites did not exhibit any signature peaks for

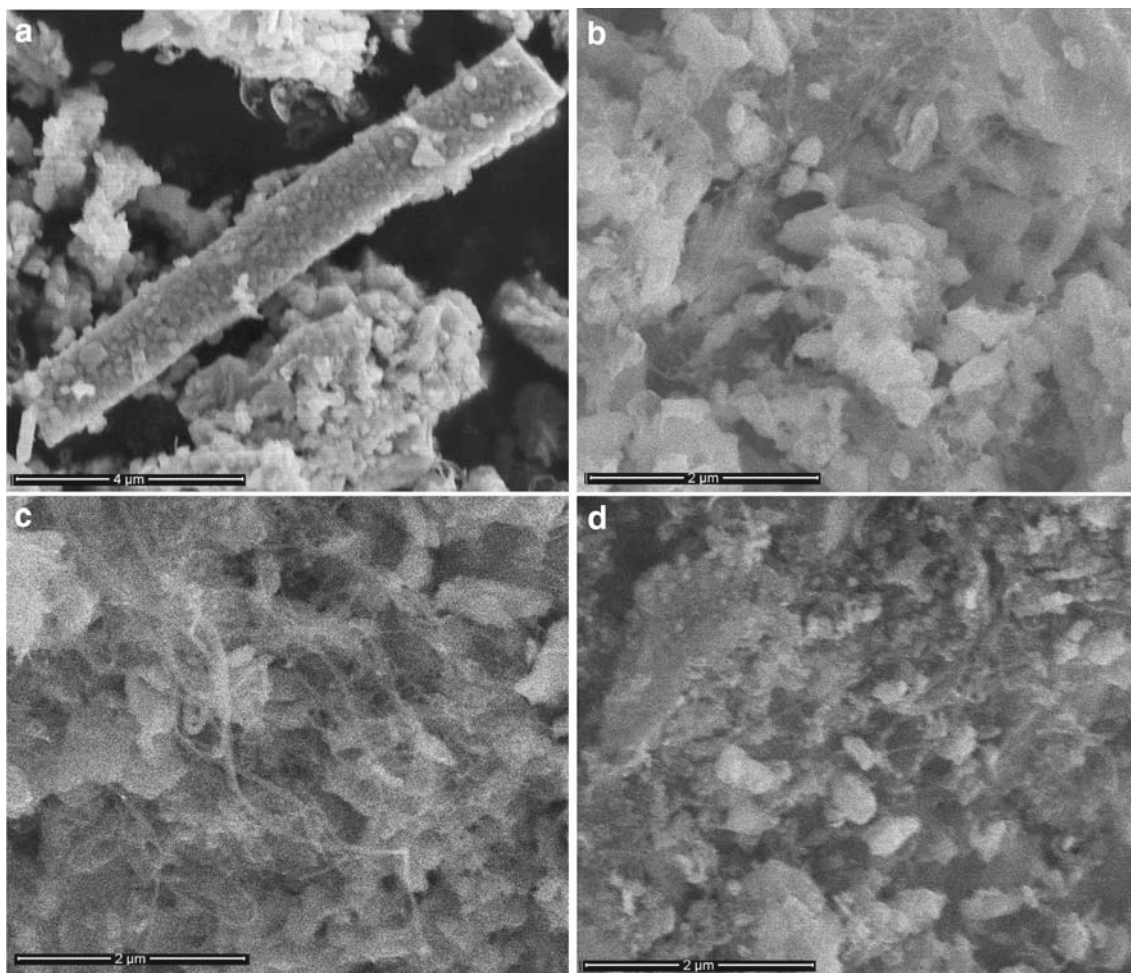


Figure 2. FESEM images of different Mo_2N composites. (a) MN, (b) MN-Fe25, (c) MN-Fe50, and (d) MN-Fe75.

functionalities on CNTs (Figure S5b in Supplementary Information).

3.1 Electrochemical studies

Hydrogen evolution reaction studies were carried out using a three electrode system in 0.5 M H_2SO_4 aqueous medium where Ag/AgCl and graphite rod were used as reference and counter electrodes, respectively. Linear sweep voltammetry (LSV) studies were carried out at a sweep rate of 5 mV/s and LSV data suggest that Mo_2N exhibit $\sim 60 \text{ mA/cm}^2$ current density at -0.4 V (Figure 4a). HER activity of Mo_2N increases when we introduced Fe into the system by making composites. As we increase the Fe content in the composites, there is enhancement in the current density. MN-Fe75 composite having higher Fe content in the composite shows highest current density of $\sim 120 \text{ mA/cm}^2$ at -0.4 V (Figure 4a). However, the onset overpotential for HER activity remained almost constant. This particularly sug-

gests that high Fe content enhances the H-desorption process which results in higher current density. From the FESEM and TEM studies, we observed that increase in the Fe content in the composite results in formation of CNTs which increases the conductivity of the composites as well as the HER activity. The control synthesis without ammonium molybdate produces only iron nitride which is not so active for HER processes (Figure S6a in Supplementary Information). Therefore, *in situ* growth of CNTs in the composites in presence of Fe, drastically enhances the HER activity. The initial high current density in these Mo_2N -based composites is due to pseudocapacitance of the material as mentioned earlier.¹⁷ There is one reduction peak just before HER process as observed in the LSV curve, due to $\text{Mo}^{\delta+}$ to Mo^0 conversion and this redox peak results in pseudocapacitance which contributes to the overall catalytic current density.

Three different reaction steps are involved in HER process:²⁵ (i) proton binds to the metal (catalyst) surface

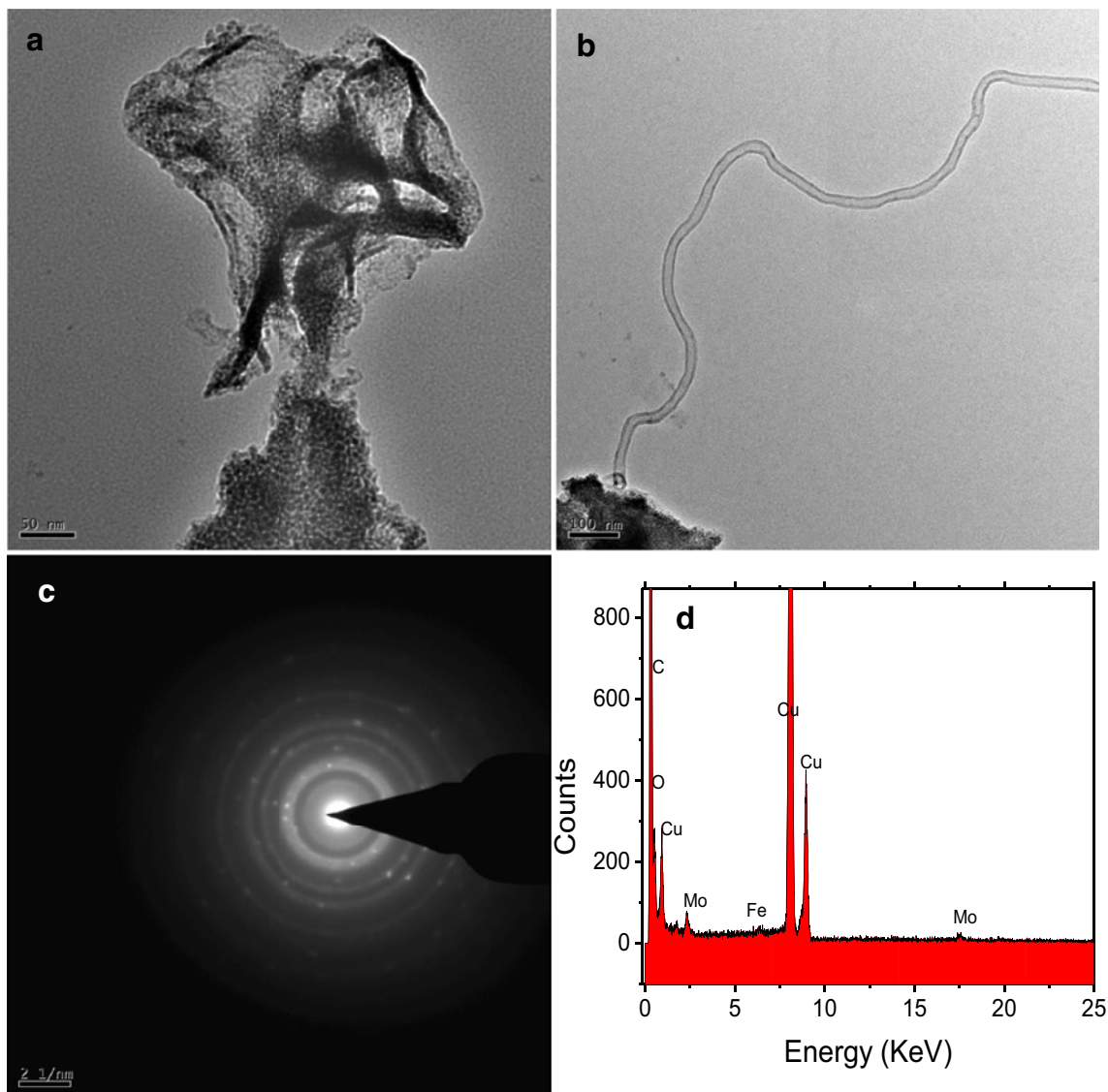
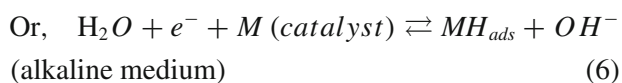
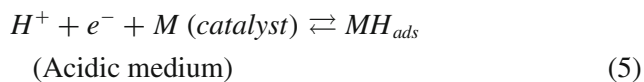


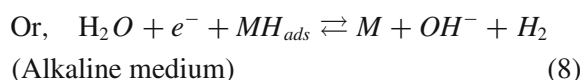
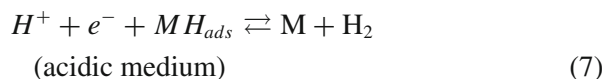
Figure 3. (a) TEM micrograph of MN-Fe50 showing aggregates of very small particles; (b) presence of CNTs in the composite; (c) electron diffraction pattern; and (d) EDAX on assembled nanostructures.

(electrochemical adsorption process, known as Volmer reaction), (ii) electrochemical desorption (Heyrovsky reaction) or (iii) chemical desorption (Tafel reaction).

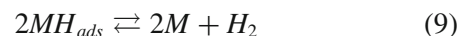
Volmer reaction:



Heyrovsky reaction:



And Tafel reaction:



Therefore, the HER process can follow either Volmer-Heyrovsky mechanism or Volmer-Tafel mechanism. The reaction mechanism can be understood from the Tafel slopes and potential dependent impedance studies.

To understand the mechanism of the HER processes, Tafel slopes were calculated from the plot of overpotential vs. Log (current density) where the slope (b) is equal to the Tafel slope and from the intercept (a), the exchange current density (J_o , at zero overpotential) can be calculated from the equation below.

$$\eta = a + b \ln J \quad (10)$$

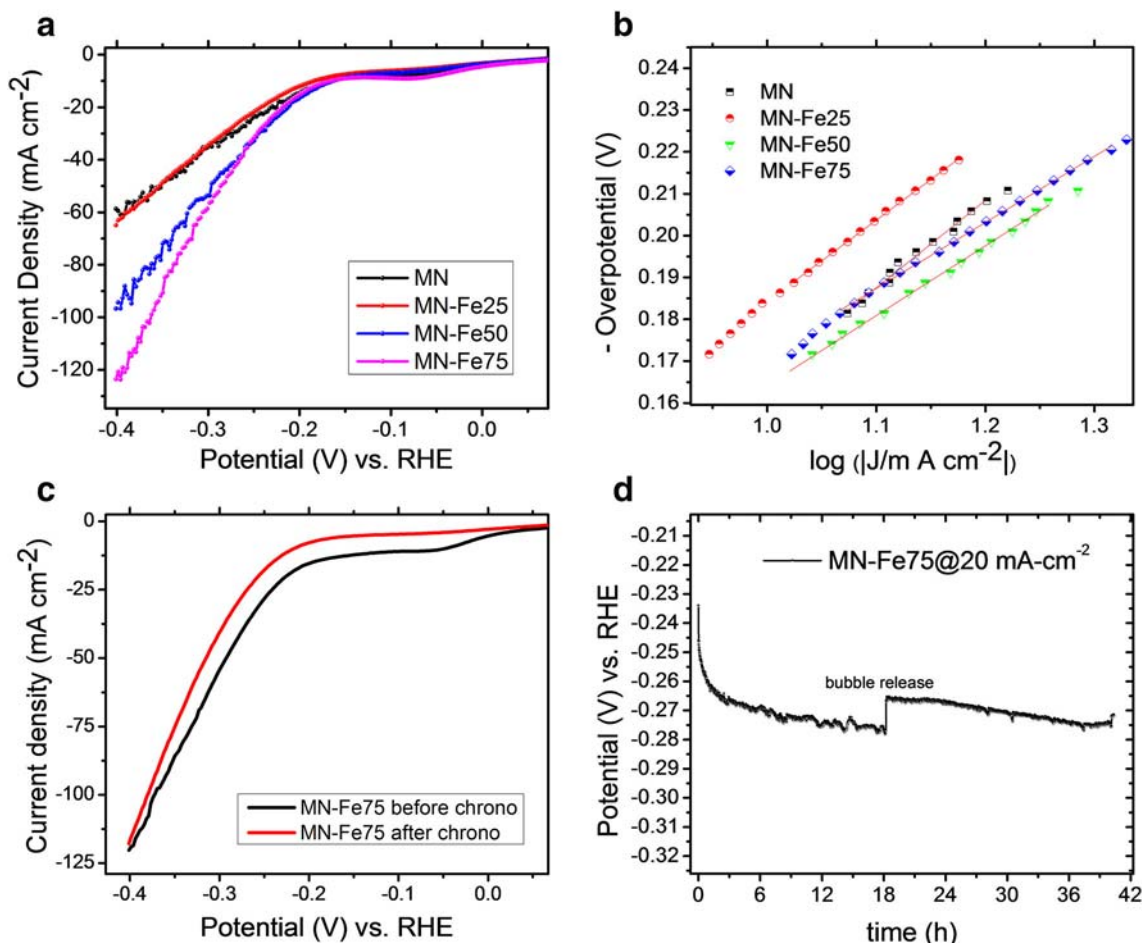


Figure 4. Electrochemical hydrogen evolution studies. (a) Linear Sweep Voltammetry curve of the composites; (b) Tafel slopes; (c) LSV curves before and after chrono studies; and (d) chronopotentiometric study of MN-Fe75 composite at an applied current density of 20 mA/cm².

Both Tafel slope and exchange current density suggest the efficiency of the catalyst for HER process. The calculated Tafel slopes from LSV data (Table S3 in Supplementary Information) suggest much higher values than the standard Tafel slopes of 120 mV/dec for Volmer reaction as rate determining step. Tafel slope is surface coverage dependent which indicates that if the surface coverage is very high, then it will have higher Tafel slope.²⁶ Therefore, prediction of the reaction mechanism using Tafel slopes is very tricky and may lead to misrepresentation of the mechanism. However, proton adsorption is weak on Mo₂N surface; therefore, higher surface coverage with proton is difficult. Now, from the LSV curve, it is evident that the enhancement of Faradaic current density is observed at much higher overpotential. Therefore, these Tafel slopes cannot help much for understanding the mechanism of the HER process.

To investigate the stability of the catalyst in acidic medium, chronopotentiometric study of MN-Fe75 were

carried out for ~40 hours at an applied current density of 20 mA/cm² and it exhibits good electrochemical stability. There is only 40 mV change in the overpotential after 40 hours of chrono studies. The LSV curve after 40 hours of chrono studies suggests that there is no change in the overall current density, *i.e.*, overall hydrogen evolution. The reduction peak at ~-0.05 V vs. RHE is vanished after chrono studies. This suggests that the contribution of pseudocapacitance to the catalytic current density is negligible. Now, the Faradaic current density is only due to hydrogen evolution reaction. We have calculated the Tafel slope from the LSV curve after chrono studies and it exhibits a Tafel slope of 131 mV/dec with an exchange current density of 0.22 mA/cm² (Figure S7 in Supplementary Information).

Figure 5 shows the cyclic voltammogram of pure Mo₂N and nanocomposites in acidic medium. The redox peaks are marked in the Figure. The peak (I) at ~0.12 V is due to the oxidation of Mo⁰ to Mo^{3+/4+}. The potential of ~0.65 V is due to the oxidation of

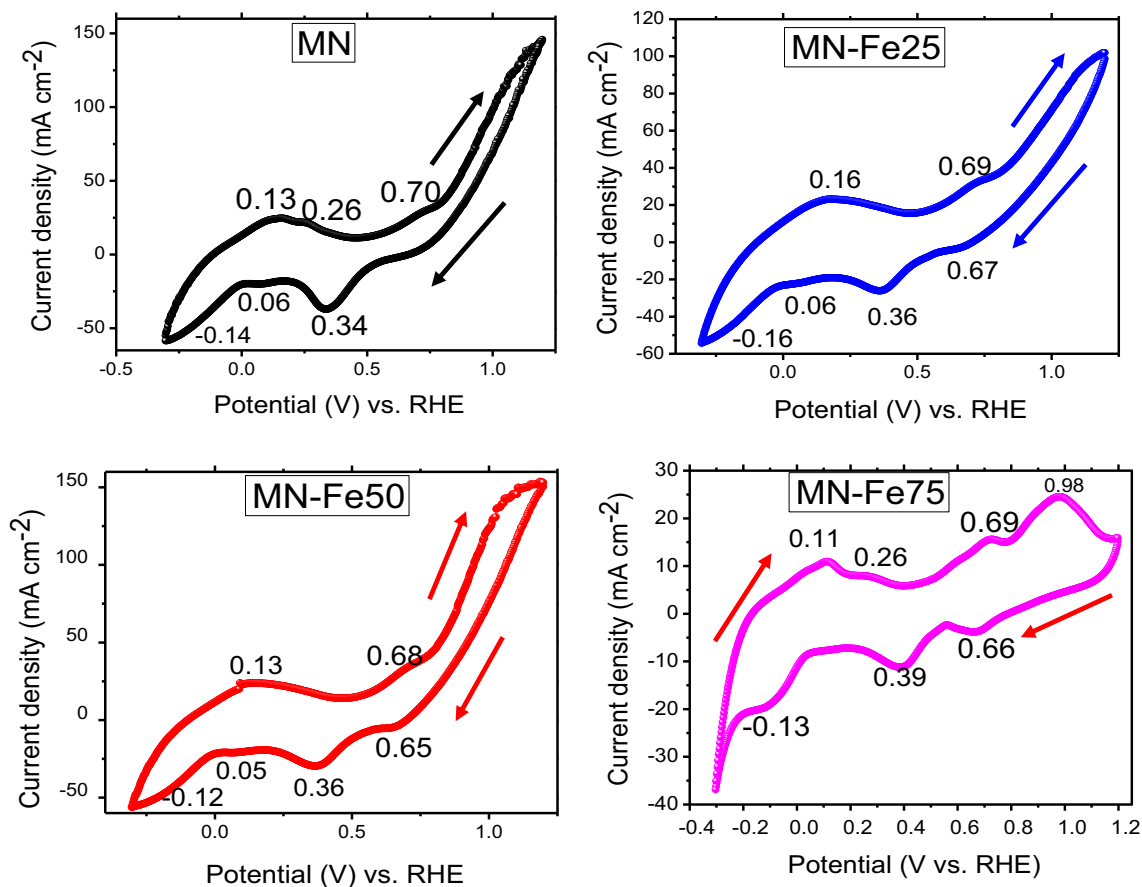


Figure 5. Cyclic voltammogram of (a) MN, (b) MN-Fe25, (c) MN-Fe50 and (d) MN-Fe75 at a sweep rate of 10 mV/s.

Mo⁴⁺ to Mo⁶⁺ (peak III). We have carried out electrochemical impedance (EIS) measurements to understand the charge transfer resistance at the electrolyte/catalyst interface during hydrogen evolution reaction. Increasing applied bias from 100 mV to 250 mV, the semicircle becomes smaller as evident from the Nyquist plot in Figure 6a. At higher applied bias, the smaller charge transfer resistance indicates higher electron mobility, *i.e.*, higher amount of hydrogen evolution. Similarly, from the Bode phase diagram, the phase angle maxima decreases at higher applied bias (Figure 6b). We have determined the resistance and capacitance values by fitting the semicircle using R_s - R_{ct} | C_{dl} equivalent circuit. However, we are unable to fit the spike at high frequency region which is generally due to instrumental wiring and electrochemical setup. This initial part (spike) at high frequency is not related to the HER process because there is no change in the impedance on applied potential. Here, low frequency region is related to the HER process and we have determined the charge transfer resistance (R_{ct}) during HER process at different applied overpotentials (Table S4 in Supplementary Information). The charge transfer resistance decreases

exponentially and the double layer capacitance initially increases and then decreases with applied overpotential. At different applied potentials, the double layer capacitance increases due to greater proton adsorption on the surface and after certain overpotential, *viz.*, 200 mV, hydrogen desorption process becomes prominent which results in decrease of the double layer capacitance (Figure 6c). We have calculated the Tafel slope as 63 mV/decade from the R_{ct} values (Figure 6d), which suggests that it follows Volmer-Heyrovsky mechanism for HER process.

We find that the composites certainly enhance the HER process in acidic media. Introducing Fe in the composite helps the formation of N-doped CNTs in the system which enhances the electrical conductivity of the composite. H-adsorption of Mo₂N surface is very weak which results in Volmer process to be the slowest step and it results in higher Tafel slope and poor HER activity. Iron nitride in the composite enhances the H-binding and facilitates the HER process on the composite surface. CNTs in the composites enhanced the overall conductivity of the composite which facilitates the electron mobility during proton reduction. Thus, the

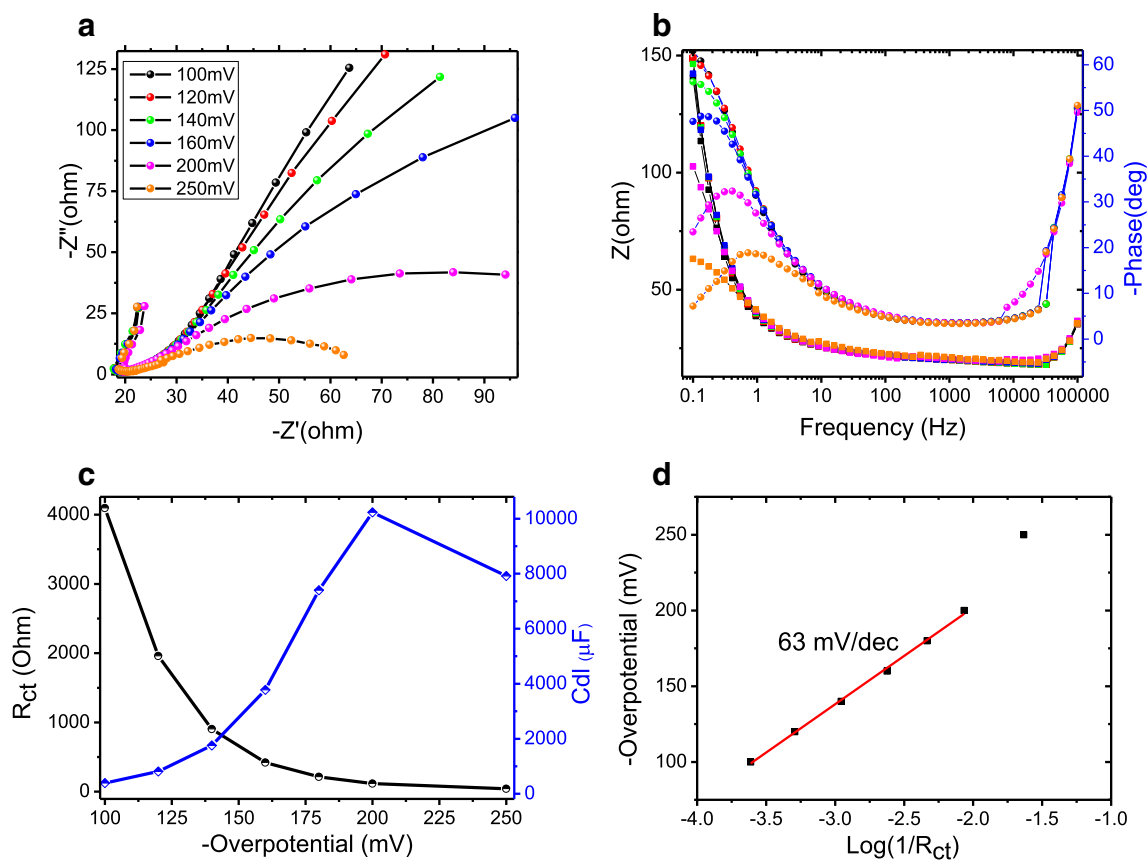


Figure 6. Electrochemical impedance spectroscopic studies showing, (a) Nyquist plot of MN-Fe75 and (b) Bode Plot of MN-Fe75 at various applied bias. (c) Charge transfer resistance and double layer capacitance at different applied potentials. (d) Tafel slope obtained from overpotential vs. $\text{Log}(1/R_{\text{ct}})$ plot.

composite materials exhibit much higher HER activity compared to bare Mo_2N and iron nitride.

4. Conclusions

Transition metal based nitride (FeN_x) composites with molybdenum nitride were synthesized where *in situ* formation of N-doped CNTs was evident. The presence of N-doped CNTs in the composites drastically enhances the electrocatalytic activity. Higher Fe content in the composite results in higher amount of N-doped CNT in the systems, which in turn results in higher HER activity with good electrochemical stability upto 42 hours in acidic medium. Synergistic effect of Mo_2N and iron nitride in the composite affects the hydrogen binding at the interface leading to higher HER activity. N-doped CNT in the composites enhances the overall conductivity of the composite facilitating the charge transfer process at the electrolyte | catalyst interface.

Supplementary Information (SI)

Figures S1–S7 and Tables S1–S3 are available in Supplementary Information at www.ias.ac.in/chemsci.

Acknowledgements

AKG thanks DST and DeitY, Govt. of India, for financial support. KO thanks UGC, Govt. of India, for fellowship.

References

- Conway B E and Jerkiewicz G 2000 Relation of energies and coverages of underpotential and overpotential deposited H at Pt and other metals to the “volcano curve” for cathodic H₂ evolution kinetics *Electrochim. Acta* **45** 4075
- Trasatti S 1972 Work function, electronegativity, and electrochemical behaviour of metals *J. Electroanal. Chem. Interfacial Electrochem.* **39** 163
- Wan C, Regmi Y N and Leonard B M 2014 Multiple phases of molybdenum carbide as electrocatalysts for the hydrogen evolution reaction *Angew. Chem. Int. Ed.* **53** 6407
- Pan L F, Li Y H, Yang S, Liu P F, Yu M Q and Yang H G 2014 Molybdenum carbide stabilized on graphene with high electrocatalytic activity for hydrogen evolution reaction *Chem. Commun.* **50** 13135
- Chen W-F, Wang C-H, Sasaki K, Marinkovic N, Xu W, Muckerman J T, Zhu Y and Adzic R R 2013 Highly active and durable nanostructured molybdenum carbide

- electrocatalysts for hydrogen production *Energy Environ. Sci.* **6** 943
- Chen W-F, Muckerman J T and Fujita E 2013 Recent developments in transition metal carbides and nitrides as hydrogen evolution electrocatalysts *Chem. Commun.* **49** 8896
 - Popczun E J, Mckone J R, Read C G, Biacchi A J, Wilttrout A M, Lewis N S and Schaak R E 2013 Nanostructured Nickel Phosphide as an Electrocatalyst for the Hydrogen Evolution Reaction *J. Am. Chem. Soc.* **135** 9267
 - Xiao P, Sk M A, Thia L, Ge X, Lim R J, Wang J-Y, Lim K H and Wang X 2014 Molybdenum phosphide as an efficient electrocatalyst for the hydrogen evolution reaction *Energy Environ. Sci.* **7** 2624
 - Mahler B, Hoepfner V, Liao K and Ozin G A 2014 Colloidal Synthesis of 1T-WS₂ and 2H-WS₂ Nanosheets: Applications for Photocatalytic Hydrogen Evolution *J. Am. Chem. Soc.* **136** 14121
 - Youn D H, Han S, Kim J Y, Kim J Y, Park H, Choi S H and Lee J S 2014 Highly Active and Stable Hydrogen Evolution Electrocatalysts Based on Molybdenum Compounds on Carbon Nanotube À Graphene Hybrid Support *ACS Nano* **8** 5164
 - Hinnemann B, Moses P G, Bonde J, Jørgensen K P, Nielsen J H, Horch S, Chorkendorff I and Nørskov J K 2005 Biomimetic Hydrogen Evolution: MoS₂ Nanoparticles as Catalyst for Hydrogen Evolution *J. Am. Chem. Soc.* **127** 5308
 - Casalongue H G S, Benck J D, Tsai C, Karlsson R K B, Kaya S, Ng M L, Pettersson L G M, Abild-pedersen F, Nørskov J K, Ogasawara H, Jaramillo T F and Nilsson A 2014 Operando Characterization of an Amorphous Molybdenum Sulfide Nanoparticle Catalyst during the Hydrogen Evolution Reaction *J. Phys. Chem. C* **118** 29252
 - Vrubel H and Hu X 2012 Molybdenum boride and carbide catalyze hydrogen evolution in both acidic and basic solutions *Angew. Chem. Int. Ed.* **51** 12703
 - Scanlon M D, Bian X, Vrubel H, Amstutz V, Schenk K, Hu X, Liu B and Girault H H 2013 Low-cost industrially available molybdenum boride and carbide as “platinum-like” catalysts for the hydrogen evolution reaction in biphasic liquid systems *Phys. Chem. Chem. Phys.* **15** 2847
 - Nørskov J K, Bligaard T, Logadottir A, Kitchin J R, Chen J G, Pandelov S and Stimming U 2005 Trends in the Exchange Current for Hydrogen Evolution *J. Electrochem. Soc.* **152** J23
 - Chen W-F, Sasaki K, Ma C, Frenkel A I, Marinkovic N, Muckerman J T, Zhu Y and Adzic R R 2012 Hydrogen-evolution catalysts based on non-noble metal nickel-molybdenum nitride nanosheets *Angew. Chem. Int. Ed.* **51** 6131
 - Ojha K, Saha S, Kumar B, Hazra K S and Ganguli A K 2016 Controlling the Morphology and Efficiency of Nanostructured Molybdenum Nitride Electrocatalysts for the Hydrogen Evolution Reaction *ChemCatChem* **8** 1218
 - Xie J, Li S, Zhang X, Zhang J, Wang R, Zhang H, Pan B and Xie Y 2014 Atomically-thin molybdenum nitride nanosheets with exposed active surface sites for efficient hydrogen evolution *Chem. Sci.* **5** 4615
 - Matanović I, Garzon F H and Henson N J 2014 Electroreduction of nitrogen on molybdenum nitride: structure, energetics, and vibrational spectra from DFT *Phys. Chem. Chem. Phys.* **16** 3014
 - Cao B, Veith G M, Neuefeind J C, Adzic R R and Khalifah P G 2013 Mixed Close-Packed Cobalt Molybdenum Nitrides as Non-noble Metal Electrocatalysts for the Hydrogen Evolution Reaction *J. Am. Chem. Soc.* **135** 19186
 - Ham D J and Lee J S 2009 Transition Metal Carbides and Nitrides as Electrode Materials for Low Temperature Fuel Cells *Energies* **2** 873
 - Ettmayer P 1970 Das System Molybdan–Stickstoff *Monatsh. Chem.* **101** 127
 - Wang S, Ge H, Sun S, Zhang J, Liu F, Wen X, Yu X, Wang L, Zhang Y, Xu H, Neuefeind J C, Qin Z, Chen C, Jin C, Li Y, He D and Zhao Y 2015 A New Molybdenum Nitride Catalyst with Rhombohedral MoS₂ Structure for Hydrogenation Applications *J. Am. Chem. Soc.* **137** 4815
 - Dyjak S, Kicinski W and Huczko A 2015 Thermite-driven melamine condensation to C_xN_yH_z graphitic ternary polymers: towards an instant, large-scale synthesis of g-C₃N₄ *J. Mater. Chem. A* **3** 9621
 - Bockris J O and Potter E C 1952 The mechanism of the cathodic hydrogen evolution reaction *J. Electrochem. Soc.* **99** 169
 - Shinagawa T, Garcia-esparza A T and Takanaabe K 2015 Insight on Tafel slopes from a microkinetic analysis of aqueous electrocatalysis for energy conversion *Sci. Rep.* **5** 13801